A thermal microjet system with tapered micronozzles fabricated by inclined UV lithography for transdermal drug delivery

2011 J. Micromech. Microeng. 21 025014

(http://iopscience.iop.org/0960-1317/21/2/025014)

IOP PUBLISHING JOURNAL OF MICROMECHANICS AND MICROENGINEERING

J. Micromech. Microeng. **21** (2011) 025014 (9pp) doi:10.1088/0960-1317/21/2/025014

A thermal microjet system with tapered micronozzles fabricated by inclined UV lithography for transdermal drug delivery

Yong-Kyu Yoon[1,5], Jung-Hwan Park[2], Jeong-Woo Lee[3], Mark R Prausnitz[3] and Mark G Allen[3,4]

[1] Department of Electrical and Computer Engineering, University of Florida, Gainesville, FL 32611, USA
[2] Department of BioNano Technology and Gachon BioNano Research Institute, Kyungwon University, Seongnam, Geonggi-do 461-701, Korea
[3] School of Chemical and Biomolecular Engineering, Georgia Institute of Technology, 311 Ferst Drive, Atlanta, GA 30332, USA
[4] School of Electrical and Computer Engineering, Georgia Institute of Technology, 791 Atlantic Drive, Atlanta, GA 30332, USA

E-mail: ykyoon@ece.ufl.edu

Received 25 August 2010, in final form 27 November 2010
Published 17 January 2011
Online at stacks.iop.org/JMM/21/025014

Abstract
Transdermal drug delivery can be enabled by various methods that increase the permeability of the skin's outer barrier of stratum corneum, including skin exposure to heat and chemical enhancers, such as ethanol. Combining these approaches for the first time, in this study we designed a microdevice consisting of an array of microchambers filled with ethanol that is vaporized using an integrated microheater and ejected through a micronozzle contacting the skin surface. In this way, we hypothesize that the hot ethanol vapor can increase skin permeability upon contacting the skin surface. The tapered micronozzle and the microchamber designed for this application were realized using proximity-mode inclined rotational ultraviolet lithography, which facilitates easy fabrication of complex three-dimensional structures, convenient integration with other functional layers, low fabrication cost, and mass production. The resulting device had a micronozzle with an orifice inner and outer diameter of 220 and 320 μm, respectively, and an extruded height of 250 μm. When the microchamber was filled with an ethanol gel and activated, the resulting ethanol vapor jet increased the permeability of human cadaver epidermis to a model compound, calcein, by approximately 17 times, which is attributed to thermal and chemical disruption of stratum corneum structure. This thermal microjet system can serve as a tool not only for transdermal drug delivery, but also for a variety of biomedical applications.

(Some figures in this article are in colour only in the electronic version)

1. Introduction

Integrated microfluidic systems have found a broad range of applications in mixing, filtering, and dispensing [1–5]. In particular, these days, interest in dispensing technologies has been greatly increased due in part to large demand for the deposition of arrayed biomolecules (DNA, peptides, and cells) for diagnosis, analysis, drug design, and other lab-on-a-chip type applications [6–8]. Such dispensing systems often borrow microjet technologies from inkjet printing systems [6, 9]. One of the concerns in a micro/nanojet system is the design and fabrication of a micronozzle to efficiently produce liquid droplets. Some research groups have introduced new nanonozzle [10, 11] and micronozzle technologies [12], and some commercial

[5] Author to whom any correspondence should be addressed.

devices adopt the microelectromechanical systems (MEMS) and complementary metal oxide semiconductor (CMOS) technologies [13–15].

While many micro/nano jet production systems in inkjet printing focus on generating high resolution and high-speed droplets, microjet systems for biomedical/chemical applications contain additional concerns and requirements depending on the specific application. In this research, a microjet system with micronozzle arrays and integrated heaters has been introduced for transdermal drug delivery and its geometry, fabrication, and performance are studied.

Ethanol is well known as a topical penetration enhancer which has been used to increase skin permeability to numerous drugs by disrupting the stratum corneum, which is the outer 10–20 μm of the skin and provides the main barrier to transdermal transport [16–18]. Another approach to increasing skin permeability involves thermal treatment of the skin [19]. Previous studies have shown the effects on either long exposures at moderate temperatures or short exposures at high temperatures. As an example of long heating at moderate temperature, exposure to 40 °C for 4 h has been reported to increase human skin permeability to a hydrophobic drug (fentanyl) by fourfold via a mechanism involving stratum corneum lipid fluidization [20]. Exposure to 80 °C for 15 s has been shown to increase porcine skin permeability to a hydrophobic compound, butanol [21].

While either ethanol exposure or thermal treatment of skin is known to increase skin permeability, the effects of their combination have not been reported. Moreover, an efficient and convenient system to generate such heated ethanol for localized transdermal drug delivery has not been developed before. Here, we are motivated to apply a transient jet of heated ethanol on skin using a micronozzle system with an integrated microheater as a new transdermal drug delivery method.

In this paper, the design, fabrication, and testing of a microheater-integrated, ethanol-loaded micronozzle jet system are detailed, and an *in vitro* test for skin permeability enhancement has been demonstrated to show its feasibility for transdermal drug delivery. The nozzle fabrication process adopts recently developed proximity-mode inclined ultraviolet (UV) lithography, which enables fabrication of the desired tapered nozzle with narrow orifice favorable for jet generation, large cavity size for liquid/drug loading, and extruded and flat nozzle top for secure skin contact, and further allows implementation of a large-scale two-dimensional (2D) micronozzle array in a batch process. The integrated ohmic heater array is utilized for vapor jet production. The increase of skin permeability and associated histological change of stratum corneum have been investigated to demonstrate potential applications of the micronozzle system. Increased skin permeability using this approach was compared with that of ethanol treatment only and thermal treatment at 70 °C only to assess the synergistic effect of our combined system.

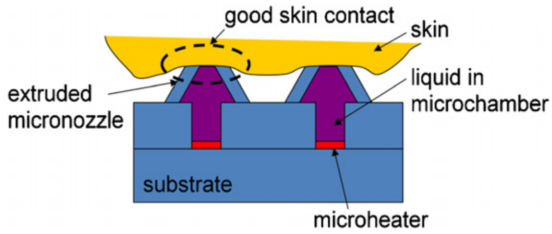

Figure 1. Schematic diagram of the microjet system for treatment of skin. A substrate contains integrated microheaters in contact with a liquid-filled microchamber. Upon activation, the liquid in the microchamber is ejected through the extruded micronozzle in direct contact with the skin. The heated ethanol microjet increases skin permeability for subsequent transdermal drug delivery.

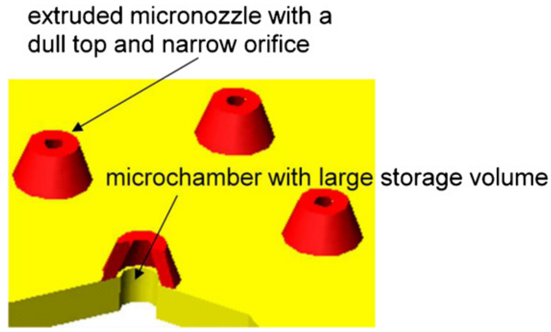

Figure 2. A three-dimensional schematic diagram of the designed micronozzle. The extruded micronozzle has a dull top and narrow orifice to facilitate skin contact and strong jet propulsion, respectively, and a microchamber with large storage volume.

2. System design and fabrication

2.1. Microjet system

The microjet system consists of an integrated microheater and a tapered hollow nozzle with a liquid loading cavity, as shown in figure 1. The microheater is used to apply highly localized thermal energy to the neighboring liquid, which increases its temperature to boiling, which results in an abrupt volume expansion. This volume change produces a pressurized vapor jet, possibly with entrained liquid, that is ejected through the small orifice of the microscale nozzle. The large cavity volume in the tapered structure is suitable for loading with microliter-quantities of liquid. Because the skin is soft and elastic, the extruded nozzle geometry is advantageous to facilitate secure contact between the nozzle tip and the skin. In contrast to, for example, a hollow microneedle [22] where the tip is designed to be sharp enough to penetrate into the skin, the tip of the microjet nozzle is designed to be dull and thereby avoid penetrating the skin as a non-invasive device. Given these design parameters, a desirable micronozzle architecture has extruded protruding, but with a dull top for good skin contact without skin penetration, a narrow orifice for strong jet propulsion, and a wide bottom cavity for large liquid loading, shown in figure 2.

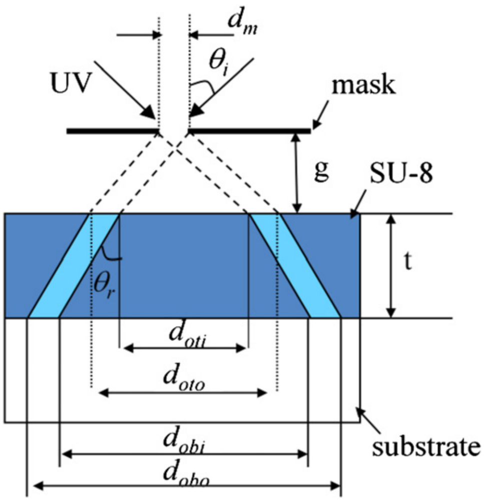

Figure 3. A schematic diagram of proximity-mode inclined UV lithography, ray trace pattern, and geometric parameters for a cross-sectional view of the micronozzle. Using this approach, a tapered structure can be easily defined in a photosensitive polymer by using an inclined UV lithographic exposure taking advantage of refraction at the polymer–air interface. See the text for definitions of the parameters shown.

2.2. Micronozzle design

The micronozzle array is fabricated using recently developed proximity-mode inclined rotational UV lithography [12]. Figure 3 shows a schematic diagram of proximity-mode inclined UV lithography, ray trace pattern, and geometric parameters for a cross-sectional view of the micronozzle. This approach is useful to make tapered structures because when the incident UV light with an incident angle θ_i in air crosses the surface of a polymer with a different refractive index, the UV light is refracted. The ray trace of the incident and refracted light can be described using Snell's law. When the refractive index of the polymer is greater than that of air, which is usually the case, the refracted angle is smaller than the incident angle, which thereby generates a tapered structure.

A clear circular pattern with a diameter of d_m in a photomask is used for proximity-mode inclined exposure where a gap of distance g exists between the photomask and the polymer film. Because the light is incident with an angle, the ray trace inside the polymer differs as a function of the gap g between the photomask and the polymer, and the polymer thickness t. For two different incident light exposures, where one is incident with a right inclination angle and the other is with a left inclination angle, the ray traces at the surface of the polymer diverge as the lights reach the bottom of the polymer film. The resultant pattern shows a tapered sidewall with a narrow upper size and a large bottom size. This is extended to the inclined rotational exposure scheme, which leads to a tapered nozzle shape with a small orifice tip and a large cavity bottom. Note that the dimensions of the nozzle orifice and nozzle height can be controlled by the gap g and the polymer thickness t as shown in figure 3 and described in equations (1)–(4):

$$d_{\text{oti}} = \frac{2 \cdot g}{\tan \theta_i} - d_m \tag{1}$$

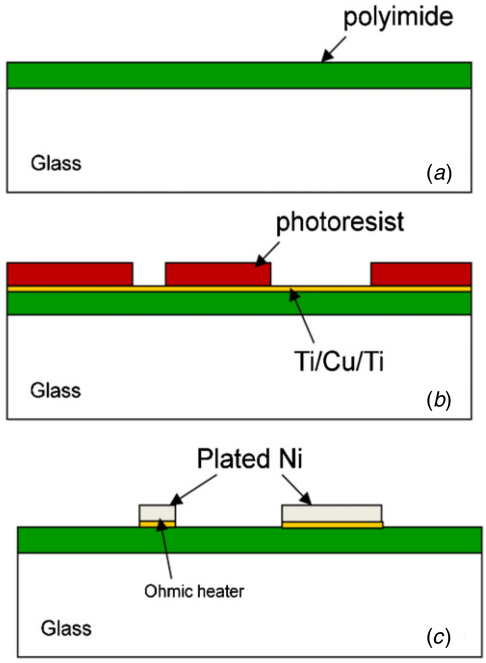

Figure 4. Fabrication process for the integrated microheater. (*a*) Polyimide layer is attached to a glass substrate. (*b*) Heater structures are micropatterned lithographically. (*c*) Ni is electroplated onto heaters to strengthen connections during heating.

$$d_{\text{oto}} = \frac{2 \cdot g}{\tan \theta_i} + d_m \tag{2}$$

$$d_{\text{obi}} = \frac{2 \cdot g}{\tan \theta_i} - d_m + 2 \cdot t \cdot \tan\left(\sin^{-1}\left(\frac{n_{\text{air}}}{n_{\text{poly}}} \cdot \sin \theta_i\right)\right) \tag{3}$$

$$d_{\text{obo}} = \frac{2 \cdot g}{\tan \theta_i} + d_m + 2 \cdot t \cdot \tan\left(\sin^{-1}\left(\frac{n_{\text{air}}}{n_{\text{poly}}} \cdot \sin \theta_i\right)\right) \tag{4}$$

where g is the gap between the photomask and the polymer surface, t is the thickness of the polymer, θ_i is the incident angle, θ_r is the refracted angle, n_{air} is the refractive index of air, n_{poly} is the refractive index of a polymer, d_{oti} is the inner diameter of the orifice tip, d_{oto} is the outer diameter of the orifice tip, d_{obi} is the inner diameter of the orifice bottom, and d_{obo} is the outer diameter of the orifice bottom.

2.3. Fabrication

The device fabrication process is divided into two parts: one for microheater fabrication and the other for micronozzle fabrication.

2.3.1. Microheater fabrication. The microheater is fabricated using UV lithography and metallization as shown in figure 4. First, a thin layer of polyimide tape (200 μm thick) with a single side self-adhesive layer is attached on a soda lime glass substrate for thermal isolation from the glass substrate (figure 4(*a*)). Note that the thermal conductivities of the soda lime glass and polyimide are 1.3 W (m^{-1} K^{-1} and 0.25 W (m^{-1} K^{-1}, respectively. A thin layer of titanium/copper/titanium (Ti/Cu/Ti, 30 nm/300 nm/30 nm) is deposited using dc sputtering on the polyimide layer. The

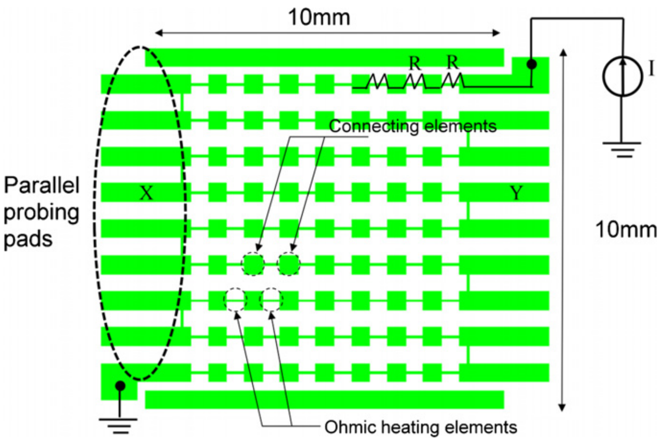

Figure 5. Schematic design of an ohmic microheater array measuring 10 mm × 10 mm. Metalized areas are shown in green. The narrow portions provide high electrical resistance and serve as the ohmic heating elements. The wide portions are low-resistance connectors between the heating elements. The parallel probing pads facilitate electrical measurements made on portions of the array.

first titanium layer is used to promote the adhesion between polyimide and copper and the top titanium layer is used for preventing copper from being oxidized during the subsequent mold patterning process. Negative tone photoresist NR 9-8000 (Futturex, Inc.) is spin coated at 2000 rpm to obtain a film of 20 μm thickness. UV light (500 mJ cm^{-2}) is exposed to pattern a thin-wire ohmic heater (see below), followed by post-exposure bake for 3 min at 75 °C and development in developer RD6 (Futturex, Inc.) for 3 min (figure 4(*b*)). After rinsing the resulting mold in DI water, the top Ti layer is etched in a dilute HF acid solution (5 volume%) and then Ni is electrodeposited through the mold up to 15 μm thickness. The Ti/Cu/Ti seed layer is time-etched in diluted hydrofluoric acid, diluted sulfuric acid (DI: H_2SO_4: H_2O_2 = 10:1:1), and diluted hydrofluoric acid in sequence (figure 4(*c*)). The thick Ni layer prevents the heated wire from being disconnected during heating due to the difference of thermal expansion coefficients of Ni and polyimide.

Figure 5 shows an array of ohmic heaters in series connection. The metal-patterned line is alternately narrow and wide, where the narrow part has high electrical resistance, serving as a localized ohmic microheater, while the wide part is a low-resistance connector between heating elements [23]. The narrow wire is designed to have a width of 100 μm, a thickness of 15 μm, and a length of 500 μm, while the wide portion has a width of 500 μm with the same thickness and length. The narrow and wide lines have a resistance ratio of 5:1. The electrical resistance of each narrow and wide line is calculated to be 23 and 4.6 mΩ, respectively. When a dc current I of 1 A is applied, the narrow and wide lines are expected to consume 23 and 4.6 mW, respectively. The overall chip has an area of approximately 10 mm × 10 mm, 80 narrow heating elements, and 63 wide connecting elements. Total power consumption is approximated to be 2.15 W for the whole chip. Note that there are extra parallel probing pads in each side, which are utilized to operate portions of the heater array. For example, the probing pads X and Y are used to apply current to energize a linear heater array between those two pads, consisting of eight heating elements and seven connecting elements, instead of operating the entire two-dimensional heater array.

When current flows, the heating elements (narrow wires) are heated more quickly than the other areas in the chip. In the array, the heaters located at the edge rows or columns will show significantly lower temperature because of relatively high heat loss at the edge of the array toward the outside of the chip compared to heating elements in the center. We therefore investigated the temperature distribution on the array using electro-thermal simulation with a multi-physics simulation tool (COMSOL package, COMSOL Inc.). Figure 6 shows the simulation results when 1 A current is applied to one end of the heater array, as the schematic describes in figure 5. Figure 6(*a*) shows an initial thermal flux distribution of ohmic heating from the current flowing through the resistive components. A large concentration of thermal flux is observed in the thin wires, as expected. In addition, a time transient simulation has been performed for the first 5 s. Figure 6(*b*) shows temperature distribution at 2.5 s, where temperature non-uniformity due to geometrical factors is observed. The overall temperature in the center is higher than that at the edge. Temperature in two spots (spot A near a center heating element and spot B near in an edge heating element) diverges after 0.25 s. But less than 0.5 s, both spots reach more than 100 °C, which is greater than the ethanol boiling temperature of 78 °C. In order to achieve uniform temperature distribution, heater design optimization could be exercised, which is not covered in this work. Also, note that this simulation does not include the heat of ethanol vaporization. In practice, the heater array is operated for up to 1 min. The heating effect longer than 30 s is not obvious and, for later experiments, the operation time is limited to 30 s.

Figure 7 shows a section of a fabricated microheater array in series connection. The width of the thin wires has been measured to be 90 μm, resulting in the increase of resistance by 10% relative to the original calculations above.

2.3.2. Micronozzle fabrication. A micronozzle array has been fabricated using inclined rotational UV lithography [12]. A dark field photomask with an array of 17 × 17 clear circular patterns and a diameter of each circle of 50 μm has been designed in a 10 mm × 10 mm area. Figure 8 shows a negative form of the photomask layout.

Figure 9 shows the fabrication process. First, 2.5 g of SU-8 (2025, Microchem, Inc.), negative tone photopatternable epoxy is dispensed on a 1 in^2 substrate with the prepatterned integrated heater array. Adhesion between polyimide and SU-8 is known to be quite poor [24, 25]. In order to improve adhesion, often the surface is treated with oxygen plasma before dispensing photoresist [26]. Here an oxygen plasma treatment has been performed in a chamber at a pressure of 70 mTorr for 30 s using a reactive ion etching system (790 RIE, Plasma Therm Inc.). It is soft baked on a hot plate at 95 °C for 5 h. Note that the hot plate and the substrate need to be maintained in level during the baking time to have a uniform SU-8 film. The photomask is then aligned on the

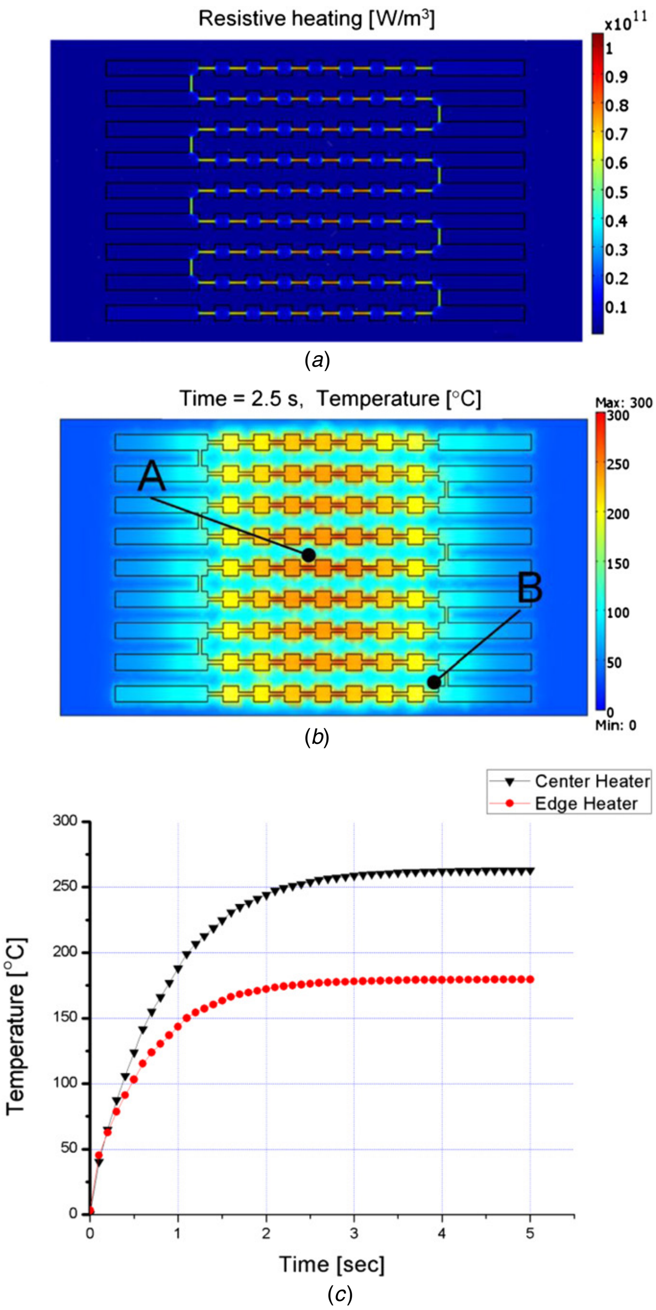

Figure 6. Electro-thermal simulation for the heater array: (*a*) thermal flux distribution upon current flow. (*b*) Temperature distribution at 2.5 s after 1 A current applied to the array. (*c*) Transient temperature at two spots (solid triangle: near the center heater A, solid circle: near the edge heater B) in the chip.

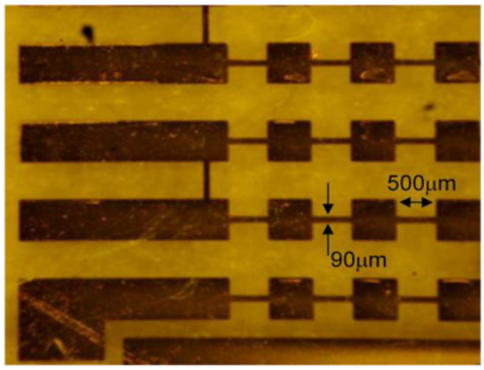

Figure 7. A section of a fabricated microheater array based on the design shown in figure 5.

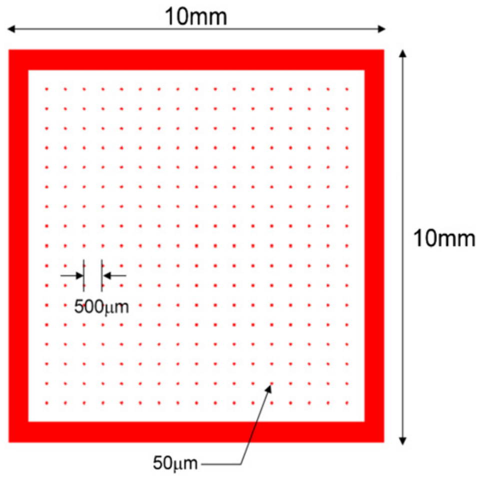

Figure 8. Photomask pattern for a micronozzle array in a negative form. Each 50 μm circle corresponds to the site of a micronozzle, with a center-to-center spacing of 500 μm.

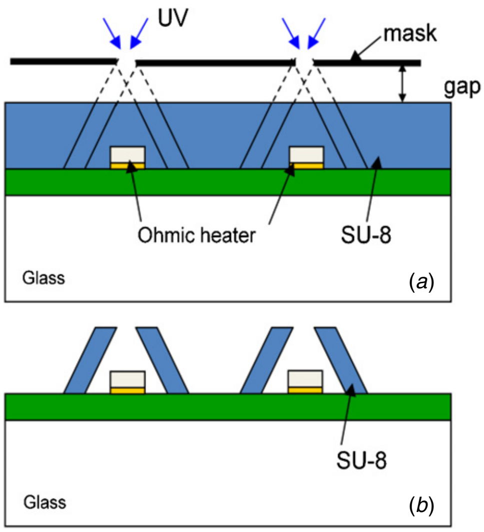

Figure 9. Micronozzle fabrication process. (*a*) Inclined rotational UV exposure through a mask to define tapered micronozzle structures in SU-8 photoresist aligned on top of ohmic heaters on a glass substrate. (*b*) Micronozzle structure after developing showing an SU-8 micronozzle on top of an ohmic heater.

SU-8-coated substrate with an air gap of 135 μm between the photomask and the polymer surface, which is followed by inclined rotational UV exposure with an inclination angle of 45° and an optical dose of 6000 mJ cm^{-2}. The moving stage is rotated in a speed of 10 rpm (figure 9(*a*)). After post-exposure bake on a hot plate at 95 °C for 1 h, the resulting structure is developed in propylene glycol methyl ether acetate (PGMEA) for 2 h (figure 9(*b*)) to complete the structure.

3. Transdermal delivery experimental materials and methods

3.1. Skin preparation

Human cadaver skin has been obtained from Emory University (Atlanta, GA, USA) with approval from the Georgia Tech Institutional Review Board (IRB) and stored at −70 °C until use. To isolate epidermis, full thickness human cadaver skin has been immersed in distilled water at 65 °C for 3 min, after which the epidermis is mechanically separated from the dermis using a spatula [27]. To isolate stratum corneum, the epidermis has been incubated at 4 °C in a solution of 0.5% trypsin in phosphate-buffered saline (PBS; Sigma-Aldrich Chemical) for 12 h, rinsed with distilled water, immersed in a fresh 0.5% trypsin solution for 3 h at 38 °C and rinsed again with distilled water.

3.2. Jet ejection of ethanol to treat skin

Hydroxy-propyl-methyl-cellulose (HPMC, Sigma-Aldrich Chemical) has been dissolved in ethanol at a concentration of 2% w/v to form an ethanol gel. To load the ethanol gel into the microchambers of the device, the prepared micronozzle array has been immersed in the ethanol gel in a vacuum chamber with a vacuum level of −30 kPa for 10 s. The residue of ethanol gel on the device surface has been gently removed by a tissue paper. Epidermis (with intact stratum corneum) has been cut into square pieces measuring up to 2.5 cm × 2.5 cm, which are mounted on a tissue paper.

To treat the skin by the ethanol jet, the prepared skin samples are placed under the ethanol gel-loaded micronozzle. To heat the ethanol gel, the integrated heater is operated by applying a constant current to the microheater for 3 s. Initially, the ethanol gel-loaded nozzle is placed on the skin in a contact mode during the heating period. The heated ethanol liquid and vapor jet impact on the elastic skin letting it be deformed for releasing the compressed liquid and vapor.

3.3. Histological examination of skin

To carry out histological analysis after treatment of the skin with the heated ethanol jet, the skin samples are covered with an optimal cutting temperature solution (Tissue-Tek, Sakura Finetechnical) and frozen with liquid nitrogen in an orientation that allows subsequent sectioning perpendicular to the skin surface. The skin samples are sectioned by a cryostat microtome (HM 560MV, Microm) at 30 μm thickness. To image changes in lipid structure of stratum corneum, cryosectioned skin samples are expanded with Sorensen Walbum buffer (0.1 M glycine, 0.1 M NaCl and 0.1 M NaOH, Sigma Chemical) for 20 min mounted on a glass slide [28], washed with deionized water, stained with Nile Red (Sigma Chemical), which is a red-fluorescent lipid stain [28], and imaged using confocal microscopy (LSM 510; Zeiss). The lipid stain has been applied using a stock solution of 0.05% (w/v) of Nile Red in acetone, which has been diluted to 2.5 mg ml^{-1} with a 75:25 (v/v) mixture of glycerol/water before use.

3.4. Transdermal delivery measurements

To determine transdermal flux quantitatively, human cadaver epidermis has been first exposed to a single application of the ethanol microjet and then a 2 cm diameter circular piece of the epidermis is mounted in a Franz diffusion chamber (PermeGear). After filling the donor and receiver compartments with PBS and incubating for 1 h to hydrate the skin at 37 °C in a water bath (Immersible multi-stirrer, Cole Parmer), the donor compartment is filled with 0.5 ml of 1 mM calcein (Sigma) and the receiver compartment is filled using approximately 5 ml of fresh PBS. After 2 h, the receptor solution is sampled for measurement of calcein fluorescence intensity using a spectrofluorimeter (QM-1; Photon Technology International). A calibration curve is used to convert fluorescence intensity into calcein concentration (detection limit was 10^{-9} M), which is used to calculate transdermal calcein flux.

Also ethanol gel was applied on human cadaver epidermis at 32 °C for 15 s and, separately, human epidermis was contacted with a hot plate at 78 °C for 15 s as control experiments to compare the change in skin permeability with the hot ethanol jet. The temperature of 78 °C was selected, because it is the normal boiling temperature of ethanol.

4. Results

4.1. Fabricated microjet system

An array of 289 micronozzles in a chip has been fabricated, among which 80 micronozzles are aligned with the ohmic heaters. Figure 10(*a*) shows a fabricated SU-8 micronozzle array integrated with microheaters, where the micronozzles and the heaters are well aligned. Figure 10(*b*) shows a scanning electron microscope (SEM) image of the micronozzle array, where a tapered orifice tip is clearly seen. The tilting angle of the orifice is approximately 25° from the vertical line to the substrate surface. The fabrication parameters and nozzle dimensions are summarized in table 1. The fabricated nozzle shows slightly different dimensions from calculated ones due to diffraction through the air gap and thick photoresist [29, 30]. The resultant wall thickness is widened by approximately 20–40 μm, while the overall shape and dimensions of the fabricated structure show good agreement with those of the designed one.

As shown in figure 11, ethanol gel with 200 cP viscosity has been successfully filled in the cavity of an array of micronozzles. The volume inside each nozzle is approximately 21 nl.

4.2. Effect of the ethanol microjet on skin permeability and stratum corneum histology

Skin permeability to a model hydrophilic molecule, calcein, has been measured after exposure to the ethanol jet. As a first control experiment, 0.006 μg of calcein was delivered across untreated epidermis (figure 12). When ethanol was applied to the epidermis at 32 °C for 15 s, there was no significant effect on skin permeability (Student's *t*-test, $P < 0.05$), which shows

Table 1. Summary of fabrication parameters and nozzle dimensions.

θ_i	θ_r	n_{SU-8}	t	g		d_{oti}	d_{oto}	d_{obi}	d_{obo}
45°	25°	1.67[a]	250 μm	135 μm	Calculated	220 μm	320 μm	453 μm	553 μm
					Measured	210 μm	330 μm	430 μm	570 μm

[a] from [12].
θ_i is the incident angle, θ_r the refracted angle, n_{SU-8} the refractive index of SU-8, t the thickness of SU-8, g the gap between the photomask and the SU-8 surface, d_{oti} the inner diameter of the orifice tip, d_{oto} the outer diameter of the orifice tip, d_{obi} the inner diameter of the orifice bottom, and d_{obo} the outer diameter of the orifice bottom.

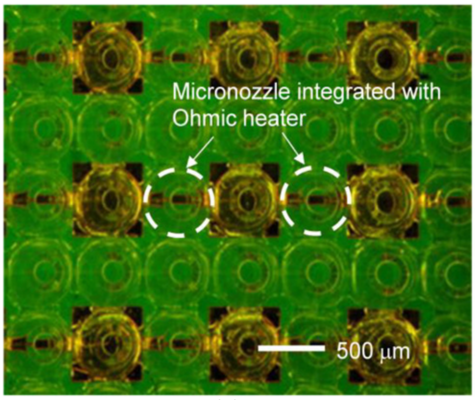

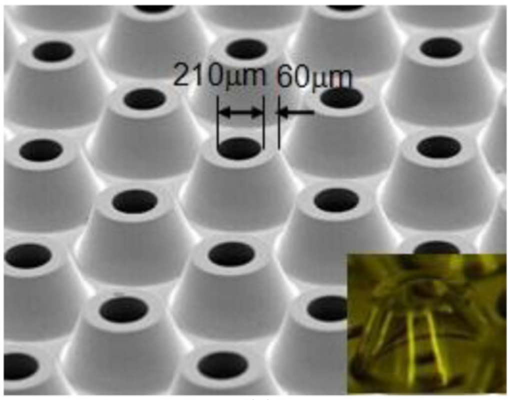

Figure 10. Fabricated micronozzle array integrated with ohmic microheaters: (*a*) optical view graph, (*b*) SEM of the micronozzle array, where $\theta_i = 45°$, $\theta_r = 25°$, $n_{SU-8} = 1.67$, $t = 250$ μm, $g = 135$ μm. Inset is an optical microscope view showing complete development inside the nozzle. In this prototype device, the micronozzles were fabricated at higher density than the microheaters. Thus, only 80 of the 289 micronozzles had microheaters aligned beneath them, a fraction of which are shown in these images. In (*a*), the green portions are micronozzles without microheaters beneath, the yellow/black portions are micronozzles with low-resistance metal connecting 'wires', and the green portions with a yellow/black stripe are the micronozzles with high-resistance ohmic heaters beneath.

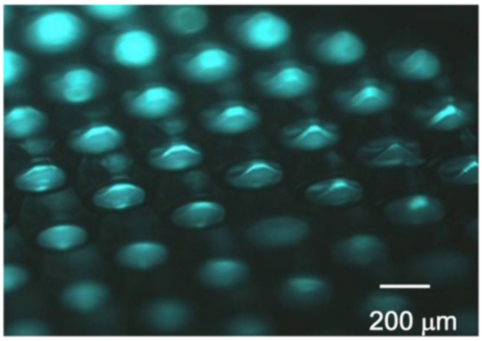

Figure 11. Optical microscopic image of a section of a microheater-integrated micronozzle array filled with ethanol gel containing 0.1% (w/w) of blue-colored curcumin to facilitate imaging.

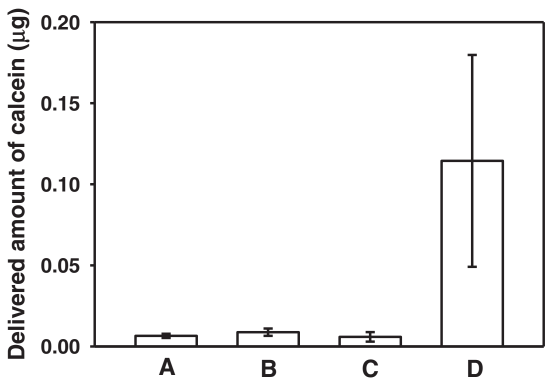

Figure 12. Effect of skin treatment on transdermal delivery of a model compound, calcein. The amount of calcein transported across human cadaver epidermis *in vitro* is shown after 2 h of delivery following (A) no treatment (negative control), (B) exposure to ethanol for 15 s at 32 °C, (C) exposure to a hot plate at 78 °C for 15 s and (D) treatment with the ethanol microjet system.

that brief exposure to ethanol has little effect on the epidermis. In another control experiment, the epidermis was heated to 78 °C for 15 s, but there was no significant effect on skin permeability ($P < 0.05$), which shows that brief exposure to elevated temperature has little effect on the epidermis. Finally, the epidermis was treated with a single application of the ethanol jet, which exposed it to a jet of high temperature ethanol for <1 s. The temperature of the jet is believed to be 78 °C, because this is the normal boiling point of ethanol. After ethanol jet treatment, 0.11 ± 0.06 μg of calcein was delivered across the epidermis, which is 17 times more than for non-treated epidermis (t-test, $P < 0.05$). This indicates that the combined effects of heat and ethanol acted synergistically to increase skin permeability. The velocity of the jet may have also played a role.

To obtain more detailed images of stratum corneum after exposure to ethanol microjet treatment, the skin has been incubated in an alkaline solution that expands the stratum corneum and then stains it with a red-fluorescent lipid stain

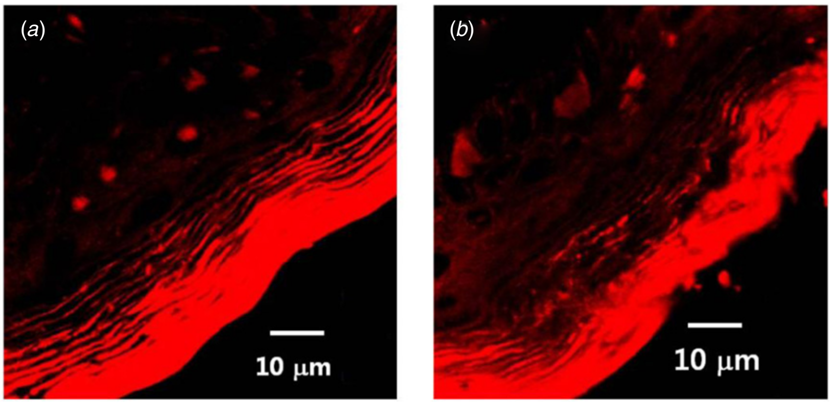

Figure 13. Confocal microscopic images of stratum corneum stained by Nile-Red. (*a*) Normal skin, showing characteristically ordered structures associated with stratum corneum lipids. (*b*) Skin treated with ethanol jet, showing disordered stratum corneum structure.

(Nile Red). Stratum corneum is the barrier layer of skin and is therefore of greatest interest to skin permeability. As shown in figure 13(*a*), untreated stratum corneum exhibits a highly ordered and aligned structure. Skin treated with the ethanol microjet appears to have a disordered stratum corneum structure, as shown in figure 13(*b*). Such stratum corneum disorder was not observed with ethanol treatment at 32 °C or thermal treatment at 78 °C (data not shown). We conclude that this stratum corneum disorder is associated with the combinatory effects of thermal treatment and chemical enhancement of ethanol vapor from the ethanol microjet and is a cause of the dramatically increased skin permeability.

5. Discussion

This paper has introduced a new application of inclined rotational UV lithography to generate an ethanol microjet system for transdermal drug delivery. The inclined exposure enabled generating a tapered structure and the rotation enabled formation of circular shapes. Especially the proximity mode inclined rotational UV lithography approach was ideally suited to fabricate tapered micronozzle structures with various advantages including the convenient formation of a micronozzle with its orifice size controlled by the gap between the photomask and the polymer substrate during the UV exposure step, the tapered angle varied by the tilting angle, and the dull tip for a non-invasive nozzle. The topside UV exposure step adopted for micronozzle patterning and the low-temperature fabrication process facilitate device integrability on top of any pre-existing devices such as the integrated heater and potentially CMOS circuitry.

The ethanol microjet system enabled a study of a novel method to increase skin permeability. Although long exposure to ethanol and long exposure to elevated temperature are each known to increase skin permeability, their combination has not been investigated before. Under the conditions used in this study, ethanol and heat alone were mild enough that they had no significant effect on the skin. However, their combination increased skin permeability by an order of magnitude. This result is significant because calcein is a moderately sized, hydrophilic molecule that is difficult to deliver across the skin. The absolute amount of calcein delivered in this study (i.e. 0.11 μg over a 2 h period) is relatively small. However, higher drug concentration on the skin surface, longer delivery time, larger skin area treated, higher microheater density and other optimization should significantly increase the absolute delivery rates. These results suggest that the ethanol microjet could be used for transdermal drug delivery applications.

6. Conclusion

Conical micronozzles integrated with microheaters were successfully fabricated using inclined rotational UV lithography and the microfabrication of thin film-resistive metal heaters for ethanol jet-enhanced transdermal drug delivery. The nozzle shape was controlled by the tilting angle, the polymer thickness, and the gap between the photomask and the substrate during proximity-mode inclined rotational UV lithography. A 2D microheater array with 80 heating elements arranged in a 1 cm × 1 cm grid was also fabricated. These heaters were integrated with the micronozzle array, such that each nozzle had a small orifice inner diameter of 210 μm, a large cavity volume of 21 nl, and an extruded height of 250 μm for skin applications. The micronozzles were loaded with ethanol gel and actuated by the integrated heater. The ethanol microjet increased skin permeability to calcein by one order magnitude by a mechanism believed to involve disruption of stratum corneum structure. The permeability increase appears to be caused by a synergistic effect of thermal and chemical effects of the heated ethanol jet. In conclusion, the inclined rotational UV lithography process provides a useful way to fabricate tapered micronozzle structures with controlled inclination angle and structure height for transdermal drug delivery and other applications.

Acknowledgments

This work was supported by Tyco Healthcare Group and EmTech Bio Seed Grant. It was also supported by Basic Science Research Program of the National Research Foundation of Korea funded by the Ministry of Education, Science and Technology (2010-0003204), and Kyungwon

University Research Fund in 2010, and National Science Foundation (CMMI 0826434) of the USA. The device fabrication and characterization and the bio tests were performed in the Georgia Institute of Technology. Numerical simulation was assisted by Mr Pit Fee Jao in the University of Florida. The authors are inventors on patents licensed to a company developing thermal ablation based products.

References

[1] Yoon Y-K, Park J-H, Cros F and Allen M G 2003 Integrated vertical screen microfilter system using inclined SU-8 structures *Proc. 16th IEEE Annual Int. Conf. on Micro Electro Mechanical Systems, 2003 (MEMS-03) (Kyoto, Japan)* pp 227–30
[2] Naher S, Orpen D, Brabazon D and Morshed M M 2010 An overview of microfluidic mixing application *Adv. Mater. Res.* **83–86** 931–9
[3] Chen L, Wang G, Lim C, Seong G H, Choo J, Lee E K, Kang S H and Song J M 2009 Evaluation of passive mixing behaviors in a pillar obstruction poly(dimethylsiloxane) microfluidic mixer using fluorescence microscopy *Microfluidics Nanofluidics* **7** 267–73
[4] Basu A S and Gianchandani Y B 2008 Virtual microfluidic traps, filters, channels and pumps using Marangoni flows *J. Micromech. Microeng.* **18** 115031
[5] Ahamed M J, Gubarenko S I, Ben-Mrad R and Sullivan P 2010 A piezoactuated droplet-dispensing microfluidic chip *J. Microelectromech. Syst.* **19** 110–9
[6] Cooley P, Wallace D and Antohe B 2002 Applications of In-Jet printing technology to BioMEMS and microfluidic systems *J. Assoc. Lab. Autom.* **7** 33–9
[7] Hoel A, Baron N, Cabodevila G and Jullien M C 2008 A microfluidic distribution system for an array of hollow microneedles *J. Micromech. Microeng.* **18** 065019
[8] Ling X, Premachandran C S, Chew M and Choong S C 2009 Development of a disposable bio-microfluidic package with reagents self-contained reservoirs and micro-valves for a DNA lab-on-a-chip (LOC) application *IEEE Trans. Adv. Packag.* **32** 528–35
[9] Beecher P *et al* 2007 Ink-jet printing of carbon nanotube thin film transistors *J. Appl. Phys.* **102** 043710–1
[10] Naik N *et al* 2007 Characterization of liquid and gaseous micro- and nanojets using microcantilever sensors *Sensors Actuators* A **134** 128–39
[11] Wang S, Zeng C, Lai S, Juang Y, Yang Y and Lee J 2005 Polymeric nanonozzle array fabricated by sacrificial template imprinting *Adv. Mater.* **17** 1182–6
[12] Yoon Y-K and Allen M G 2006 Proximity mode inclined UV lithography *Solid-State Sensor, Actuator, and Microsystems Workshop (2006)* pp 98–9
[13] Koo B, Kim D, Moon H, Kim J, Jung E, Kim J-Y, Jin Y, Lee S and Kim J 2009 4″ E-ink active-matrix displays based on ink-jet printed organic thin film transistors *Presented at 9th Int. Meeting on IMID (IMID 2009)* 1631–3
[14] Kabalnov A, Rolly L and Gondek J. 2005 9-ink printing using vivera inks: image quality and permanence on photo and visual arts media *Proc. Int. Conf. Digit. Printing Technol.* 364–70
[15] Chwalek J M *et al* 2002 A new method for deflecting liquid microjets *Phys. Fluids* **14** 37–40
[16] Cornwell P A and Barry B W 1995 Effects of penetration enhancer treatment on the statistical distribution of human skin permeabilities *Int. J. Pharm.* **117** 101–12
[17] Walters K A, Brain K R, Dressler W E, Green D M, Howes D, James V J, Kelling C K, Watkinson A C and Gettings S D 1997 Percutaneous penetration of *N*-nitroso-*N*-methyldodecylamine through human skin *in vitro*: application from cosmetic vehicles *Food Chem. Toxicol.* **35** 705–12
[18] Brand R M, Jendrzejewski J L, Henery E M and Charron A R 2006 A single oral dose of ethanol can alter transdermal absorption of topically applied chemicals in rats *Toxicol. Sci.* **92** 349–55
[19] Mitragotri S 2006 Temperature dependence of skin permeability to hydrophilic and hydrophobic solutes *J. Pharm. Sci.* **96** 1832–9
[20] Shomaker T S, Zhang J and Ashburn M A 2000 Assessing the impact of heat on the systemic delivery of fentanyl through the transdermal fentanyl delivery system *Pain Med.* **1** 225–30
[21] Flynn G L, Behl C R, Linn E, Higuchi W I, Ho N F and Pierson C L 1982 Permeability of thermally damaged skin V: permeability over the course of maturation of a deep partial-thickness wound *Burns Incl. Therm. Inj.* **8** 196–202
[22] Wang P-C, Wester B A, Rajaraman S, Paik S-J, Kim S-H and Allen M G 2009 Hollow polymer microneedle array fabricated by photolithography process combined with micromolding technique *IEEE EMBC Conf.* pp 7026–9
[23] Yoon Y-K and Allen M G 2001 Pt Heater/sensor microarray for distributed fluidic cooling assessment *Proc. 2001 ASME IMECE* p 23894
[24] Agirregabiria M, Blanco F J, Berganzo J, Arroyo M T, Fullaondo A, Mayora K and Ruano-Lopez J M 2005 Fabrication of SU-8 multilayer microstructures based on successive CMOS compatible adhesive bonding and releasing steps *Lab Chip* **5** 545–52
[25] Arroyo M T, Fernandez L J, Agirregabiria M, Ibanezl N, Aurrekoetxea J and Blanco F J 2007 Novel all-polymer microfluidic devices monolithically integrated within metallic electrodes for SDS-CGE of proteins *J. Micromech. Microeng.* **17** 1289–98
[26] Shenton M J, Lovell-Hoare M C and Stevens G C 2001 Adhesion enhancement of polymer surfaces by atmospheric plasma treatment *J. Phys. D: Appl. Phys.* **34** 2754–60
[27] Hobson D W 1991 *Dermal and Ocular Toxicology: Fundamentals and Methods* (Boca Raton, FL: CRC Press)
[28] Kleene N K, Pickens W L and Wang T F 2001 Visualization of the lipid barrier and measurement of lipid pathlength in human stratum corneum *AAPS Pharm. Sci.* **3** 1–9
[29] Thompson L F, Wilson C G and Bowden M J (eds) 1994 Organic resist materials—theory and chemistry *Introduction to Microlithography* (Washington, DC: American Chemical Society)
[30] Yoon Y-K, Park J-H and Allen M G 2006 Multidirectional UV lithography for complex 3D MEMS structures *J. Microelectromech. Syst.* **15** 1121–30